MODFLOW-2000 FOR CYLINDRICAL GEOMETRY WITH INTERNAL FLOW OBSERVATIONS AND IMPROVED WATER TABLE SIMULATION

Tom Clemo

Center for the Geophysical Investigation of the Shallow Subsurface

Boise State University

Boise, Idaho 83725-1536

Technical Report BSU CGISS 02-01

August, 2002

Abstract

A modified form of the MODFLOW-2000 code provides a tool to estimate a hydraulic conductivity distribution near a borehole. The modified code allows the effects of wellbore screen intervals, screen clogging, and disturbed zone skin to be taken into account. The primary application has been in an investigation of electromagnetic borehole flow meter measurement interpretation.

MODFLOW-2000 was modified to simulate a two-dimensional cylindrical geometry. The two dimensions are vertical and radial with angular symmetry. The geometry is similar to the RADMOD preprocessor to MODFLOW, but is more flexible in that the grid spacing in the radial direction may be non-regular and the hydraulic conductivity of a layer need not be constant. This modification includes sensitivity calculations so that parameter estimation can be performed.

To support parameter estimation using flow meters, a new measurement category of internal flow observations was introduced. Internal flow observations occur at locations that are fully contained within the model domain. The standard MODFLOW-2000 code is limited to flow observations across the model domain boundaries. The new internal flow measurement observations are compatible with the normal MODFLOW-2000 Cartesian geometry and with the cylindrical geometry modifications.

A third modification moves the node location of a cell containing the water table from the center of the cell to the location of the water table. The vertical position of the node dynamically follows changes in the water table position. This change improves the simulation of water table dynamics for both cylindrical geometry and Cartesian geometry simulations.

Together these modifications provide a tool for modeling pumping from a wellbore with multiple screened zones in a layered aquifer with an azimuthally uniform disturbed zone. If the wellbore is included, the pumping rate can be applied to the upper node of the wellbore. The flow into or from the formation is correctly apportioned in the model. Thus, the modeler does not have to apportion flow into individual layers, a difficult procedure in the case of a disturbed zone that results in a positive skin effect.

Contents

List of Tables

List of Figures

1 Introduction

The finite-difference formulation for cylindrical geometry used by the RADMOD code (Reilly and Harbaugh, 1993) provides a capability to simulate radial flow to a well. However, RADMOD lacks the flexibility to simulate radial variation in hydraulic conductivity caused by clogged well screens or formation disturbances near the borehole. We need this flexibility to an investigate the influence of such heterogeneity on wellbore flow profiles created from electromagnetic borehole flow meter measurements.

Briefly, an electromagnetic borehole flow meter measures the voltage drop across an annulus, created by ions moving through a magnetic field imposed in the annulus by the flowmeter. The voltage drop is used to determine the axial flow velocity within a borehole (Young and Pearson, 1995). The net inflow to the well over an interval can be estimated by calculating the difference in vertical flow measured at the two ends of the interval. From the net inflow one can deduce estimates of the hydraulic conductivity distribution of the formation near the borehole. Common practice at this time is to assume a perfectly layered formation resulting in conductivity estimates proportional to the ratio of inflow rates to the borehole (Molz et al., 1994). At the Boise Hydrogeophysical Research Site, BHRS (Barrash et al., 1999), we believe that the wellbore screens may be partially clogged with sand resulting in a lower hydraulic conductivity through the screen compared to the formation. Our initial investigations using a thermal simulator, QUICKFIELD (Tera Analysis, 1999), revealed that clogging causes a distortion of the flow into a wellbore compared to the flow in a layered formation, potentially biasing the interpretation of electromagnetic flowmeter measurements.

We decided to replace QUICKFIELD in our analysis because a lack of access to the source code makes it cumbersome to integrate into an analysis scheme and because we felt a fluid flow simulator would be more readily accepted by the hydrologic community. Of the readily available non-commercial software we examined, RADMOD, and the similar capabilities of RADFLOW (Johnson et al., 2002), came the closest to fulfilling our needs. However, we could not specify the hydraulic conductivity of the screen to be different from that of the formation. We would also have to base the geometry of the formation on the geometry of the screen, which would have led to a large model. We chose to modify MODFLOW-2000 (Harbaugh et al., 2000; Hill et al., 2000) rather than RADMOD because of usefulness to us of the inversion capability of MODFLOW-2000. This report is limited to the modifications that were made to MODFLOW-2000. The investigation of electromagnetic borehole flow meter interpretation will be documented separately.

With our modified version we can include the open wellbore explicitly in our simulations of electromagnetic flow meter measurements. In order to provide simulated measurements within the borehole, a new observation type

was needed. The 2001 version of MODFLOW-2000 can be used to simulate observations of flow across the model domain boundaries, but not internal flows that do not cross a boundary. So, we added an internal flow observation type. The internal flow observation capability is fully integrated with the other observation types and could be used independently of the other modifications described in this report.

While benchmarking the transient behavior of the cylindrical geometry modifications, the poor response of the model near the water table was noted. RADMOD provides a better simulation of water table dynamics than we achieved with our initial modifications. Examining the RADMOD code revealed that the outer nodes are located at the domain boundaries in a RADMOD model. Having nodes on the model edge is incompatible with MODFLOW-2000 but is compatible with earlier versions of MODFLOW using the General Finite-Difference Package. General Finite-Difference Package allows more flexible model geometry compared to standard MODFLOW. RADMOD is a preprocessor that supplies an input file for the General Finite-Difference Package. As we show below, dynamically positioning the node of a finite-difference cell at the water table leads to a more accurate simulation of water table dynamics.

Since our objective was to create a tool for our investigation of borehole flow meter measurements, we have not attempted to make the cylindrical geometry model compatible with all of the MODFLOW-2000 packages. While we hope to completely integrate the cylindrical geometry model into MODFLOW-2000, we will not do so unless the USGS expresses an interest. The current limitations of our modifications are listed in Section 5 of this report.

The exact coding changes made to MODFLOW-2000 do not belong in this report. However, the changes may be of interest to its readers. We provide Internet access to these modifications through http://cgiss.boisestate.edu/cgiss_pub.html. The file is accessible through the listing of this technical report, CGISS 02-01. The file is a compressed tape archive (tar) file. The compression was performed using Gnu's gzip utility. The file contains all the modified, and unmodified, files needed to compile the code. A file for the make utility is also supplied. UNIX diff command output files, in directory diff, contain just the changes made to Version 1.7 12/04/2001 of MODFLOW-2000. In addition, the tar file includes the two test cases described in Sections 2.3 and 4.4.1. Finally, this report is included. The file contents may be updated in the future to reflect corrections and additional compatibility improvements.

2 Cylindrical Geometry

2.1 Formulation

2.1.1 Conductance

The description of modifications made to support cylindrical geometry follows the development of the RADMOD code by Reilly and Harbaugh (1993). The modification differs from RADMOD with the relaxation of the use of a constant grid-expansion factor. In this section, we assume the reader has some familiarity with MODFLOW, but not necessarily with RADMOD. Figure 1 depicts the finite-difference discretization in cylindrical geometry. The model domain is composed of a series of annular rings about a common central location. The modified code accommodates constant layer thicknesses, ΔZ, and arbitrary radial spacing, ΔR. (Variable layer thickness might also be simulated correctly, but has not been investigated.) In the figure, the lines separate finite-difference cells. For a few cells, the cell computational nodes are shown as dots. The location of a cell boundary is specified by the radial coordinate sr. The radial position of a node location is designated r, as shown for the last column in the figure. The inner domain boundary of the model may be the central axis (sr_1=0.0) or at some radial distance away from the axis.

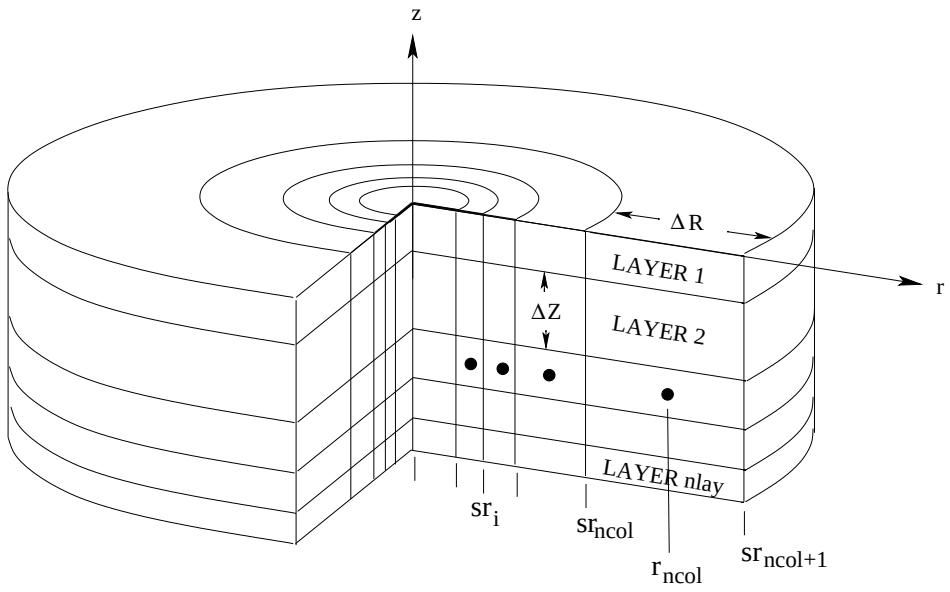

Figure 1: Finite-difference discretization for cylindrical geometry.

Each cell in a model is assigned a set of constant properties. The MODFLOW codes transform the cell's assigned hydraulic conductivity or transmissivity into hydraulic conductance terms between nodes. Hydraulic conductance includes the geometry of the finite-difference cells in the determination of the effective ability to transmit flow between

nodes. The basic equation for conductance is

$$C = \frac{KA}{L} \tag{1}$$

where: K is hydraulic conductivity, A is the area of the common boundary between cells and L is the distance between nodes. Reilly and Harbaugh present the hydraulic conductance in the radial direction between two nodes in cylindrical geometry as

$$C_r = \frac{K_r 2\pi\Delta z}{ln\left(\frac{r_{i+1}}{r_i}\right)} \tag{2}$$

where: K_r is the hydraulic conductivity between the nodes located at radii of r_i and $r_{i+1}$and Δz is the axial thickness of the layer. The nodes are the "centers" of two adjoining cells. The cell "center" is the radial location that separates the cell into two halves of equal cross sectional area normal to the vertical direction, rather than the location with equal distance from the edges of the cell. Equation 2 is based on constant hydraulic conductivity within each layer.

In our case, we have constant hydraulic conductivity within each cell, but each cell may have a different hydraulic conductivity. Therefore, we calculate conductance for each half cell between the center node and the cell boundary for adjacent cells and then add the two half cell conductances in series. For the two half cell conductances we have

$$C_{r_i} = \frac{K_{r_i} 2\pi\Delta z}{ln\left(\frac{sr_i}{r_i}\right)} \tag{3}$$

and

$$C_{r_{i+1}} = \frac{K_{r_{i+1}} 2\pi\Delta z}{ln\left(\frac{r_{i+1}}{sr_i}\right)}$$

where, sr_i is the boundary between cell i and cell $i+1$. The conductance between the nodes becomes

$$C_r = \frac{C_{r_i} C_{r_{i+1}}}{C_{r_i} + C_{r_{i+1}}} \tag{4}$$

Note that if $K_{r_i} = K_{r_{i+1}} = K_r$ then (4) is equivalent to (2).

Continuing to follow Reilly and Harbaugh, the cell "centers" are located such that the cross-sectional areas normal to the z axis of the two half cells are equal. The two half cells are: 1) less than the center position, and 2) greater than the center position.

$$\pi\left(r_i^2 - sr_i^2\right) = \pi\left(sr_{i+1}^2 - r_i^2\right) \tag{5}$$

Thus,

$$r_i = \sqrt{\frac{1}{2}\left(sr_i^2 + sr_{i+1}^2\right)} \tag{6}$$

Whereas RADMOD uses a constant expansion ratio to define sr, we use the standard MODFLOW spacing along rows, DELR, to define the cell boundaries. One absolute position, the radius of the inner boundary of the first column, is also required to fully define the sr values. The definition of the vertical conductance follows directly from (1) with the definition of cross-sectional area as

$$A_i = \pi \left(sr_i^2 - sr_{i+1}^2 \right) \tag{7}$$

2.1.2 Conductance and the Sensitivity Process

The inversion capability of MODFLOW-2000 requires the determination of the sensitivity of observations to parameters. By the chain rule of calculus the sensitivity of observations to parameters can be calculated as the sensitivity of the observations to conductance multiplied by the sensitivity of the conductance to the parameters. The required modification of the MODFLOW-2000 sensitivity process is quite limited because the sensitivities of the observations to conductance remain unchanged.

As an example, consider an internal flow observation that is defined as the radial flow from cell i to $i+1$. The observation can be written as

$$Q_o = C_r \left(h_{i+1} - h_i \right) \tag{8}$$

The sensitivity to a hydraulic conductivity parameter, b, is

$$\frac{\partial Q_o}{\partial b} = \frac{\partial C_r}{\partial b} \left(h_{i+1} - h_i \right) + C_r \left(\frac{\partial h_{i+1}}{\partial C_r} - \frac{\partial h_i}{\partial C_r} \right) \frac{\partial C_r}{\partial b} \tag{9}$$

The terms $\frac{\partial h}{\partial C_r}$ do not require modification for cylindrical geometry. We only need to provide a calculation of $\frac{\partial C_x}{\partial b}$, where x represents either the vertical or radial direction. By the chain rule

$$\frac{\partial C_r}{\partial b} = \frac{C_{r_{i+1}}^2}{\left(C_{r_i} + C_{r_{i+1}} \right)^2} \frac{\partial C_{r_i}}{\partial b} + \frac{C_{r_i}^2}{\left(C_{r_i} + C_{r_{i+1}} \right)^2} \frac{\partial C_{r_{i+1}}}{\partial b} \tag{10}$$

with,

$$\frac{\partial C_{r_i}}{\partial b} = \frac{2\pi \Delta z}{ln\left(\frac{sr_i}{r_i} \right)} \text{ , and } \frac{\partial C_{r_{i+1}}}{\partial b} = \frac{2\pi \Delta z}{ln\left(\frac{r_{i+1}}{sr_i} \right)} \tag{11}$$

Likewise,

$$\frac{\partial C_{v_i}}{\partial b} = \frac{A_i}{\frac{1}{2}\left(\Delta z_u + \Delta z_l \right)} \tag{12}$$

where, u and l refer to the thickness of the upper layer and lower layers respectively.

2.1.3 Storage Terms

The storage terms are simply volume, V_i, times specific storage, S_s,

$$\begin{aligned} SS_i &= S_s V_i \\ &= S_s A_i \Delta z \end{aligned} \tag{13}$$

or area, A_i, times specific yield, S_y, in the case of unconfined layers.

$$SY_i = S_y A_i \tag{14}$$

where A_i is defined by (7). The sensitivities of storage terms to specific storage parameters or specific yield parameters are the volume or area respectively.

2.1.4 Horizontal Flow Barriers

The horizontal flow barrier package allows a thin low permeability zone to be incorporated into the model without having to explicitly represent the geometry of the zone. For a borehole flowmeter investigation, the horizontal flow barriers can be used to simulate well casing and to represent clogging of the wellbore screen. Within MODFLOW-2000, the barrier is treated as a conductance at the boundary between cells that is added in series to the horizontal conductance. The data input for a horizontal barrier is in the form of hydraulic conductivity divided by the barrier thickness, K/L, hence the thickness need not be explicitly defined. The conductance of the barrier, C_b, is the cross-sectional area normal to the flow direction multiplied by the data input.

$$C_b = A_b \cdot (K/L) \tag{15}$$

In the radial flow case, the cross-sectional is $A_b = 2\pi\, sr_i\, \Delta z$, replacing DELR$\cdot\Delta z$ or DELC$\cdot\Delta z$ for both the flow and sensitivity processes.

2.2 Implementation

The cylindrical geometry option is specified by setting the conductance-averaging flag, LAYAVG, in the LPF file to 3 for all layers. Setting LAYAVG to 3 for some but not all of the layers will generate an error message. In addition, if the cylindrical geometry option is used, the option XSECTION must be set in the BAS6 file. The radial distance of the innermost boundary is read from a file type CGEO, IUNIT(50), as specified in the name file. (See Appendix

A.1). The radial distance of the innermost boundary is the only datum in this file. Consistent with the XSECTION specification, the DELR array in the DIS file is used to specify radial cell widths. In the DIS file, the number of rows, NROW, must be set to 1 and the width of the columns, DELC, must be set to 1.0. No automated error checking of NCOL or DELC is provided.

Four internal variables are calculated within MODFLOW-2000 to implement the cylindrical geometry option. These are the radial conductance, CR, the vertical conductance, CV, the cell hydraulic capacity, SC1, and, for convertible cells, the cell water table yield, SC2. The calculations of all of these variables are controlled by a new subroutine called SGWF1LPF1RADIAL that has been added to the gwf1lpf1.f file. The cross-sectional areas and cell node radial positions are also calculated and stored within SGWF1LPF1RADIAL using the ALLOCATEABLE variable attribute. Thus, compilation of the modified code is limited to FORTRAN 90 and 95 compilers. The advantage of isolating these calculations and variables within the SGWF1LPF1RADIAL subroutine is that perturbation of the standard MODFLOW-2000 code is limited.

A second subroutine, SSEN1LPF1RADIAL, is used to calculate the derivatives of CR, CV, SC1, and SC2 with respect to parameters. This subroutine is also called by the horizontal flow barrier package to obtain cross-sectional areas normal to the radial direction. As in the SGWF1LPF1RADIAL subroutine, the cross-sectional areas normal to the vertical direction and the cell node positions are calculated and stored. This small duplication of storage space is inefficient but limits the perturbation of the original code.

2.3 Testing

We follow Reilly and Harbaugh's (1993) lead by using the test case presented in the RADMOD documentation: flow to a partially penetrating well in a homogeneous aquifer of infinite extent with anisotropic hydraulic conductivity. The WTAQ3 (Barlow and Moench, 1999) numerical implementation of an analytic solution (Moench, 1997) for a homogeneous water-table aquifer response to pumping from a partially penetrating finite-diameter well was used to define the reference drawdown. Moench's analysis is an extension of the analytical solution (Neuman, 1974) that was used to benchmark the RADMOD preprocessor. The reference case includes pumping from a 25 foot interval at the bottom of a 100 foot thick homogeneous aquifer of infinite extent. The aquifer has a horizontal hydraulic conductivity of 100 ft/day and a vertical hydraulic conductivity of 10 ft/day. The transmissivity, T, of the aquifer is 10,000 ft^2/day. The specific storage is $5.x10^{-6}$ per ft and the specific yield is 0.2. A pumping rate, Q, of 125,670 ft^3/day is used, which makes the dimensionless drawdown equivalent to the drawdown in units of feet. The well has a radius of 0.936 ft.

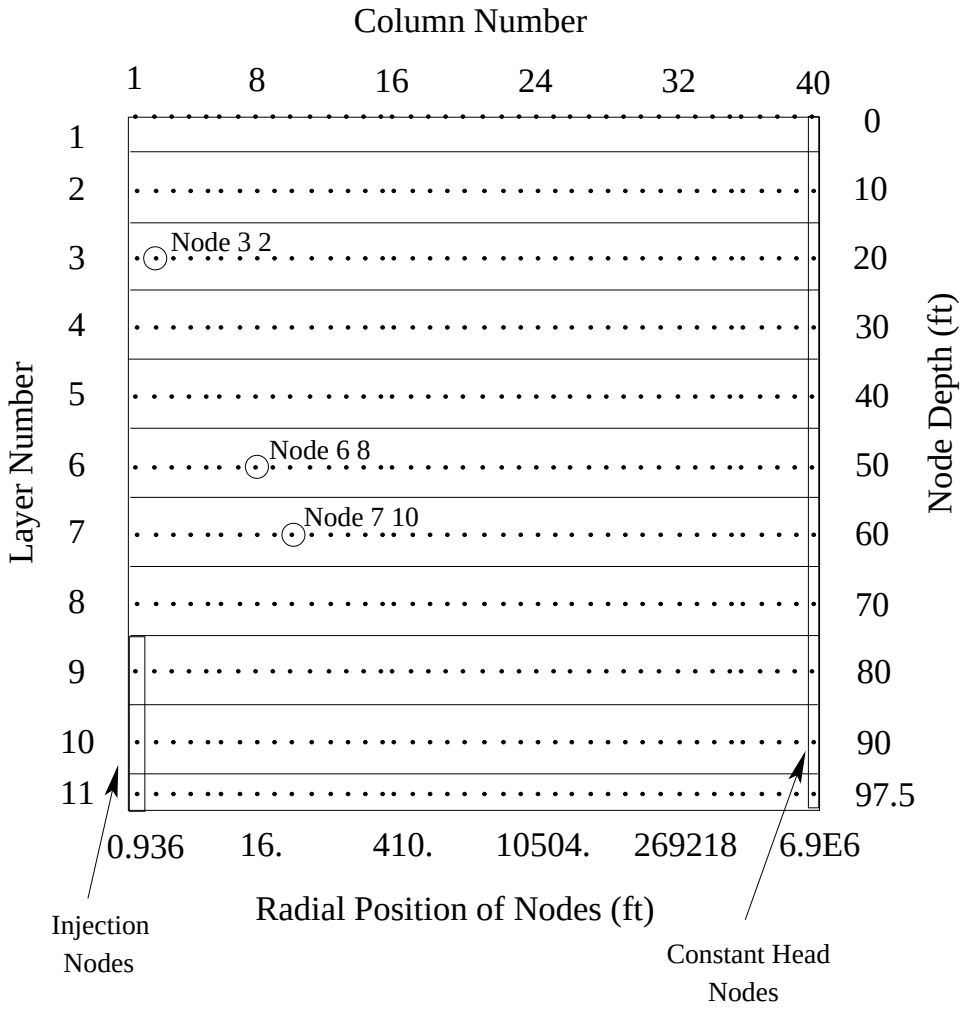

Figure 2: Schematic of test model for cylindrical geometry.

Note that the horizontal axis is a logarithmic scale. The dots represent node positions. They are spaced evenly along the log axis. After (Reilly and Harbaugh, 1993).

As shown in Figure 2, the test case has 11 layers and 40 columns. The radial position of the nodes increases exponentially with a constant growth multiple of 1.5. In Figure 2, the layer numbers are indicated on the vertical axis and the column numbers are shown above the drawing. Note that the horizontal axis is drawn with a logarithmic scale making the nodes appear to have equal separation. The nodes used to simulate pumping withdrawal are the three lower nodes of Column 1, shown in the lower left within a box. The pumping rate is apportioned between these nodes by the thickness of the layers. Three nodes, at locations Layer 6 Column 8, Layer 7 Column 10, and Layer 3 Column 2, are circled. The calculated drawdown at these nodes is used to compare the cylindrical geometry results

with the WTAQ solution.

To prepare for the test case, RADMOD was modified to report the radial separation distance between cell boundaries. RADMOD output was then used as the DELR input data. Changes were made to the RADMOD model in that the node closest to the axial center is the center of a cell. Thus, the innermost boundary of the MODFLOW-2000 model is located at a radial distance of 0.708 rather than 0.936, which positions the nodes of column 1 at the same position in both models. Likewise, the last nodes of the last column are positioned at the center of the column, thus extending the outer boundary of the model. An inconsequential impact of these differences is that the vertical cross-sectional area for flow is larger for the first and last columns, resulting in reduced drawdown near the well during the first second of pumping.

We have retained the positioning of the nodes at the top layer along the top boundary, at least at the beginning of the pumping period. The MODFLOW-2000 code has been modified so that the location of the node in a cell that contains a water table is dynamically positioned at the water table. Section 4 describes in detail the rationale for positioning of the upper nodes at the water table. The change has a significant impact on the model performance. The nodes in Layer 11, the bottom layer, are located at the center of the layer in the MODFLOW-2000 model rather than the lower boundary as in the RADMOD model. In the MODFLOW-2000 model, the nodes of the bottom layer are closer to the nodes of the neighboring layer by 2.5 ft compared to the separation distance of the RADMOD model. As with the changes to Columns 1 and 40, we believe that this change has little effect on the simulation.

Figure 3 presents the comparison of dimensionless drawdown calculated for the three highlighted nodes of Figure 2. The MODFLOW-2000 calculations are shown as dashed lines, with the WTAQ calculations as solid lines. The dimensionless drawdown is calculated from dimensional drawdown as

$$D_d = \frac{4\pi T}{Q} s \tag{16}$$

where s is the drawdown in units of feet. The abscissa is dimensionless time - calculated as

$$T_d = \frac{Tt}{S_s r_{6,8}^2} \tag{17}$$

where: t is the time in days, S_s is storativity, $5x10^{-4}$, and $r_{6,8}$ is 16 ft, the radial position of the node located at Layer 6 Column 8. The comparisons reveal a slight under-prediction of drawdown by MODFLOW-2000.

The modified MODFLOW-2000 code allows wellbore dynamics to be simulated, which is not possible using the RADMOD preprocessor. The test case was changed so that the first column of the model represents the wellbore. For this new case, the location of the inner boundary is the z axis (sr_1=0.0 ft) and the location of the boundary

between the first and second column is 0.936 ft. The hydraulic conductivity of the wellbore, Column 1, was set to an arbitrarily large value of 10^{11}ft/day. The specific storage of the cells in column one was reduced to $6.0\text{x}10^{-10}$ per ft and the specific yield was increased to 1.0. The horizontal flow barrier package was used to simulate the impermeable borehole casing by introducing a 10^{-8} per day conductance barrier between the first and second column of layers 1 through 8. The WEL file was changed to specify pumping of the entire 125,670 ft^3/day from Layer 5, Column 1. Layer 5 was chosen because a drawdown of 40 ft occurs in the well, causing the upper three layers of the wellbore to go dry. In the WTAQ input, the simulation was changed from an infinitesimal well to a well with an 0.936 ft inside radius.

Figure 4 presents the dimensionless curves for each of the three comparison locations. The WTAQ calculations for an infinitesimal radius pumping well are drawn as dotted lines. The solid lines are for the finite dimensional wellbore and the dashed lines are from the MODFLOW-2000 simulations.

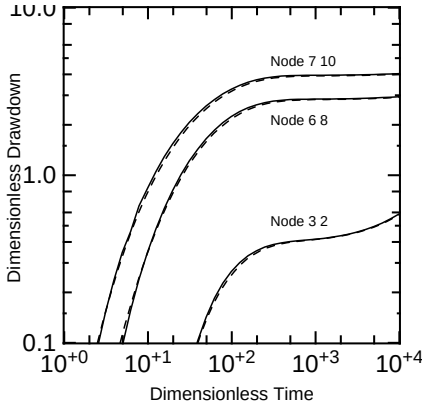

Figure 3: Comparison of cylindrical geometry model (dashed) to WTAQ calculations (solid).

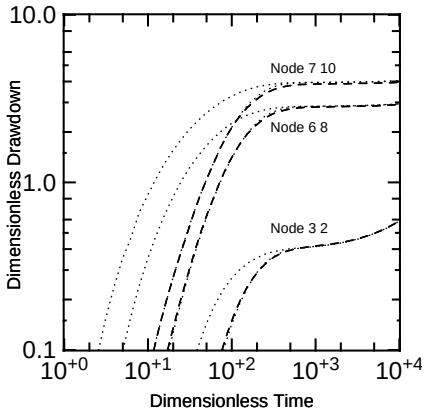

Figure 4: Comparison of drawdown with wellbore storage.
The solid lines are WTAQ results, dashed lines are MODFLOW-2000,
and the dotted lines are from WTAQ without wellbore storage

3 Internal Flow Observations

3.1 Introduction

Internal flow observations are calculations of the flow between cells of the model. Groups of cells may be defined to specify flow across long cross-sections through a model. This could be used as an alternative to calculating flow through portions of a model from the cell-by-cell flow file. The internal flow observation calculations are performed in double precision so the internal flow observations may be more accurate than post-processing of the MODFLOW results. Our use is in conjunction with the cylindrical geometry model to simulate borehole flow meter measurements.

The code modification for the internal flow observations is distinct from the cylindrical geometry modification. Internal flow observations do not require the use of cylindrical geometry nor are the internal flow observations required to use cylindrical geometry.

3.2 Formulation

Internal flow observations are the sum of flows crossing specific cell boundaries. The flow is calculated as

$$Q_i = C_{xi} * (h_i - h_j) \tag{18}$$

where C_{xi} is the conductance in the row, column, radial, or vertical direction between contiguous cells i and j, and h_i is the hydraulic head in the cell.

The sensitivity of the internal flow observations to parameter changes is

$$\frac{\partial Q_i}{\partial b} = \frac{\partial C_{xi}}{\partial b}(h_i - h_{i+1}) + C_{xi}\left(\frac{\partial h_i}{\partial b} - \frac{\partial h_{i+1}}{\partial b}\right) \tag{19}$$

Equation 9 described the same sensitivity in terms of $\frac{\partial C_x}{\partial b}$.

3.3 Implementation

Internal flow observations are activated by supplying a data file designated as type FLOB in the name file. The format of the data follows that of the general head boundary observations but is not identical. Internally within the code, the existence of internal flow observations is recognized by the non-zero status of variable IUNIT(42). A set of subroutines following the structure of the general head boundary observations is supplied in file obs1flw1.f. The subroutine naming convention is followed, with FLW substituted for GHB. The data storage of the internal flow

observations has been integrated with the other flow observations. It is assumed that the internal flow observations are the last type of flow observations added to the list of observations. This may need to be changed if additional flow observation types are added to the code.

Formal input instructions for the internal flow observations are included in Appendix A.2. The input differs slightly from the general head boundary observation input because the internal flow observations require the designation of two cells rather than a single cell. Item 5 of the input has been changed so that seven data items are read for each component of an observation group. The layer, row, and column of the receiving cell are given first. The direction of flow is defined so that flow toward the receiving cell is positive. Next, the layer, row and column of the discharging cell are listed. Positive flow is away from the discharging cell. The seventh data item read is the weight factor. The weight factor is a multiplying factor to allow a fraction of the flow between individual cells to contribute to the flow measurement. The weight factor provides a correction factor if the location of the flow measurement does not coincide perfectly with the cell geometry. For example, if the grid size is larger than the measurement interval, then a fraction of the flow from cell to cell should be calculated. If the desired flow occurred along some interior line of a cell, then a weighted average of the flow across the cells boundaries might be used. Multiple cell pairs may be specified for an individual flow observation. The consistency of each cell pair is checked to ensure that they are adjacent. No automated check of the continuity of multiple cells in an observation is performed.

3.4 Example: Borehole Flow Meter Observation

Figure 5 depicts the region near the pumped section of the second test case of section 2.3. The figure shows the innermost four columns and bottom five layers. In this test case, the borehole is explicitly included in the simulation as shown by the cross-hatching of Column 1. A thick line separating Columns 1 and 2 of Layers 7 and 8 depicts the casing simulated by an effectively impermeable horizontal flow barrier. The three circled regions highlight the cell boundaries we now use to represent borehole flow meter measurement locations.

In the FLOB file, we specify 18 internal flow observations, composed of one cell pair for each of the three locations. Observations are requested at five times, one per decade of dimensionless time from 1.0 (1.1 s) to 10^4 (0.13 days). The early times occur while decrease in wellbore storage is reducing flow into the borehole from the formation. At later times, the influence of wellbore head decline on flow into the borehole has become negligible.

At the location identified as EBF-2 in Figure 5, the receiving cell of the observation is identified as Layer 9, Row 1, and Column 1. The discharging cell is identified as Layer 10, Row 1, and Column 1. Thus, positive flow is defined as upward within the borehole. A weighting factor of 1.0 is used because both a flow meter measurement and the internal flow observation should account for all the flow in the borehole.

Figure 6 presents the simulated measurements for the three locations identified in Figure 5. The upper curve, EBF 1, includes all the flow from the formation. The small flows initially indicate almost the entire response to pumping is a decrease in the water level in the wellbore. As time progresses, a larger fraction of the pumping is made up of formation fluid. After a dimensionless time of 10^3 the water level in the wellbore has stabilized such that nearly all of the pumping rate is made up by formation fluid, providing confirmation that the measurement calculation is correct.

If we inspect the late time flow rates, we see that 19% of the flow into the wellbore occurs from layer 11, 38% from Layer 10, 43% from Layer 9. In the first test case, the pumping withdrawal was apportioned between Layers 9, 10, and 11 based on the thickness of the layers, resulting in a flow split of 20%, 40%, and 40% respectively. Figure 6 suggests the assumed flow split was in error. Obviously, Figure 3 indicates that the error was not significant. The discrepancy highlights a potential use of the cylindrical geometry model: determining relative pumping rates into layers of a multilayer well for use in larger regional-scale simulations.

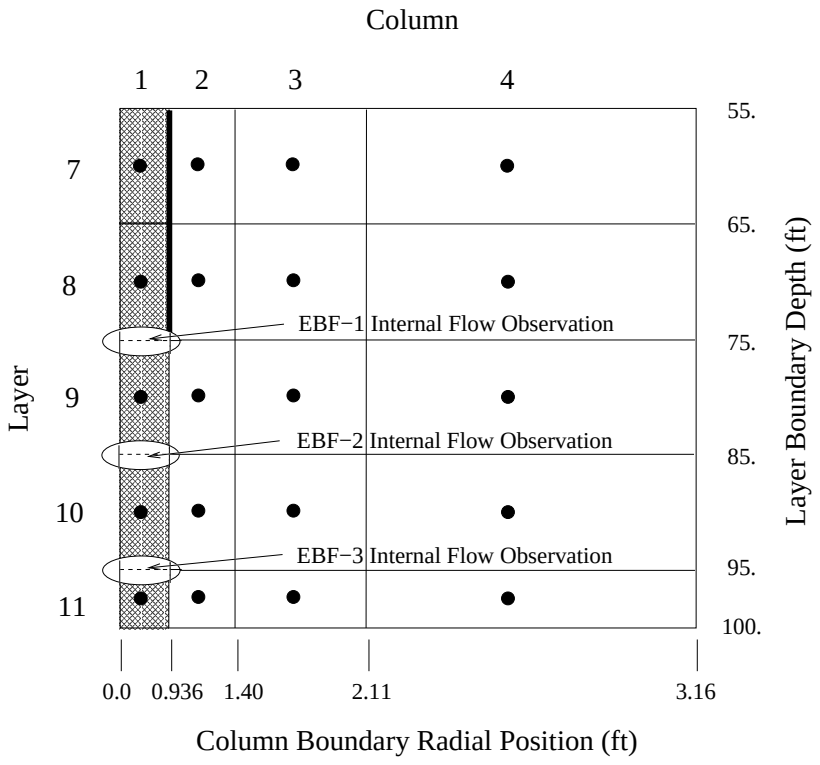

Figure 5: Detail of Internal Flow observation locations

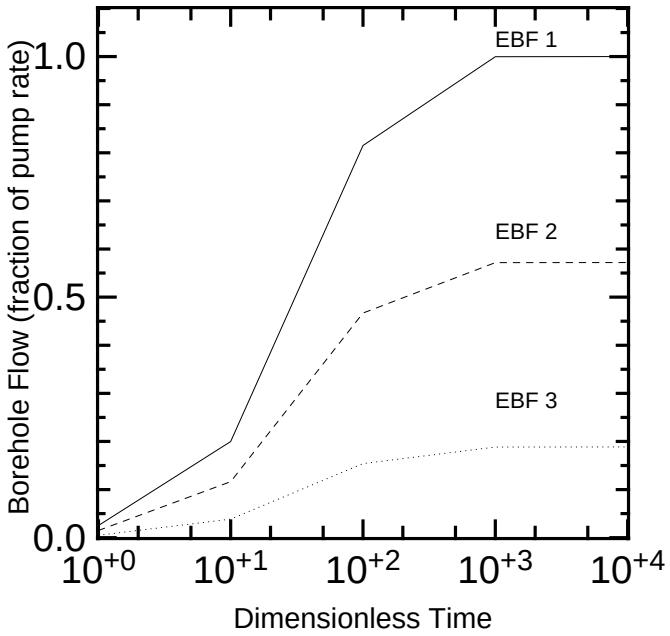

Figure 6: Normalized flow at the internal flow observation locations.

The locations are defined in Figure 5.

4 Incorporation of Water Table Movement into a Block-Centered Finite-Difference Model

4.1 Introduction

In this section, we demonstrate that simulation of fluid flow near a water table is improved if the node of a cell that contains the water table is located at the water table rather than at the center of the cell. The location of the node should dynamically follow the water table. MODFLOW-2000 uses the water table elevations to calculate the hydraulic conductance but not to position the node location. Since the water table elevations are already available, a minor change to the code results in improved performance.

To properly develop the sound rationale for our modification, we need to review some of the fundamentals of the finite-difference formulation of groundwater flow that we avoided earlier by stressing the relation of the cylindrical geometry modification to the RADMOD code. MODFLOW is based on a three-dimensional block-centered finite-difference formulation. The subsurface is divided into a set of contiguous cells. The flow properties of each cell are specified by a set of hydrologic parameters. The equations of flow through the subsurface are approximated

by finite-difference equations that use a single head value to describe the fluid pressure associated with a cell. The equations are formed using the assumption that the head exists at a specific location, the cell's node. The term block-centered indicates the node is located at the center of the cell.

4.2 Block-Centered Finite-Difference Formulation

The equation for saturated flow in terms of hydraulic head, h, is

$$S_s(x,y,z)\frac{\partial h(x,y,z)}{\partial t} = \frac{\partial}{\partial x}K(x,y,z)\frac{\partial h(x,y,z)}{\partial x}+\frac{\partial}{\partial y}K(x,y,z)\frac{\partial h(x,y,z)}{\partial y}+\frac{\partial}{\partial z}K(x,y,z)\frac{\partial h(x,y,z)}{\partial z}+Q(x,y,z) \quad (20)$$

where: S_s is specific storage, K is hydraulic conductivity, and Q is a fluid source or sink. A finite-difference model is a discretization of the flow equation where the head is only calculated at a finite number of locations. Material properties are considered constant within cells. Figure 7 shows nine cells of a block-centered finite-difference model. The figure represents a vertical cross-section, of thickness Δc into the page, with elevations given by the z coordinates, and horizontal location given by r. The circles are cell nodes.

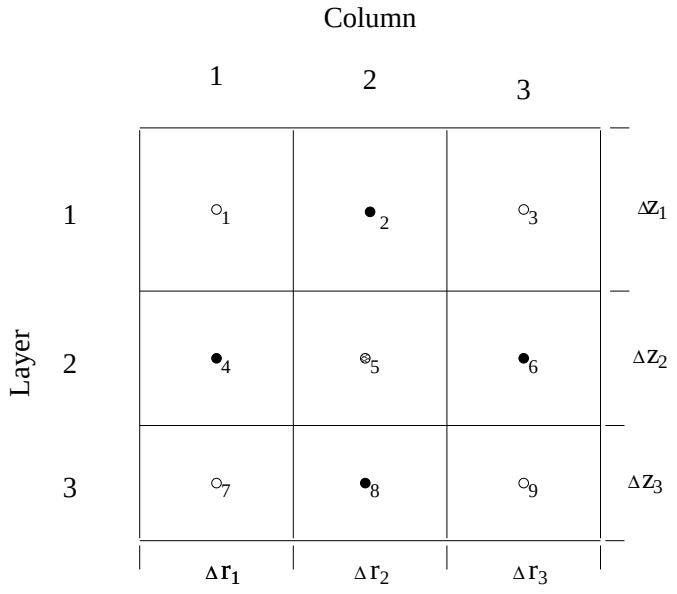

Figure 7: Example block-centered finite-difference grid.

Dots and circles represent node positions.

The nodes represented as dots are in hydraulic contact with the center node.

The nodes depicted as open circles are not.

To form the finite-difference equations, the filled nodes are considered to be in hydraulic contact with the center cell. The cells in contact diagonally, open circles, do not connect hydraulically to the center cell. The gradient is calculated by treating the hydraulic head of a cell to be located at the node, the center of the cell. Fluid flow between two cells is, in effect, one dimensional. The one dimensional flow is converted to volumetric flow by multiplying by the area of the contact face between cells. In Figure 7 the contact area between nodes 5 and 6 is $\Delta c \Delta z_2$. The flow into the face from node 5 is the same as the flow out of the face to node 6.

$$Q_{56}^{+} = Q_{56}^{-} \tag{21}$$

$$\Delta c \Delta z_2 K_{x5} \frac{(h_{56} - h_5)}{\frac{\Delta r_2}{2}} = \Delta c \Delta z_2 K_{x6} \frac{(h_6 - h_{56})}{\frac{\Delta r_3}{2}} \tag{22}$$

$$CR_5 (h_{56} - h_5) = CR_6 (h_6 - h_{56}) \tag{23}$$

where: Q_{56} represents the flow across the contact face of cells 5 and 6; K_r is the hydraulic conductivity in the r direction; h_{56} is the head at the interface of the cells 5 and 6; and CR, using the MODFLOW convention, is the cell conductance in the r direction. Eliminating h_{56} from (23) we get

$$Q_{56} = \frac{CR_5 CR_6}{CR_5 + CR_6} (h_6 - h_5) \tag{24}$$

$$= CR_{56} (h_6 - h_5) \tag{25}$$

where CR_{56} is the conductance between nodes 5 and 6 as in (4).

Integrating over the cell volume, the left hand side of (20) is approximated by

$$S_s \Delta c \Delta r \Delta z \frac{\Delta h_i}{\Delta t} = SS_i \frac{\Delta h_i}{\Delta t} = S_i \frac{\Delta h_i}{\Delta t}$$

where S_s is the specific storage of the cell material, and S_i is the capacitance of the cell. Specific storage represents the change in void space within the aquifer that occurs in response to a change in the fluid pressure. As the head increases the load that must be supported by the aquifer material decreases. The aquifer expands slightly in response to decrease in load creating additional void space for fluid storage. The discretized flow equation for an internal cell is

$$S_i \frac{\Delta h_i}{\Delta t} = \sum_{j=1}^{N} C_{xij} (h_j - h_i) + Q_i \tag{26}$$

where: subscript x is a meta character that becomes r, c, or, v for flow between columns, rows or layers respectively;

N is the number of neighboring cells, 4 for two-dimensions and 6 for three dimensions; and Q_i may account for flow sources or sinks to the node in addition to fluid flow through the aquifer.

Having developed the finite-difference flow equation for internal nodes, we turn to a cell that represents the top layer of an unconfined aquifer. Fluid flow in the unsaturated portion of the aquifer is approximated by two terms, Q_i to represent recharge and S_y to represent the effects of changing water table elevation. S_y accounts for the change in fluid occupied void space within the cell for a change in water table elevation. Typically, in a fully saturated flow code such as MODFLOW, the dynamics of water movement within the capillary fringe are ignored by treating the change in occupied void space to be instantaneous. S_y can be approximated as

$$S_y = (\Theta - \Theta_r)$$

where Θ is porosity and Θ_r is residual saturation of the aquifer material. As the change in water table elevation is equivalent to the change in h_i, the capacitance of a water table cell becomes

$$S_i = (S_s \Delta z + S_y)\, \Delta y \Delta r \tag{27}$$

$$S_i \backsimeq S_y \Delta c \Delta r = SY_i \tag{28}$$

$S_s \Delta z$ has been dropped in (28) because it is usually negligibly small compared to S_y.

It is important to keep in mind that a typical fully saturated code approximates the water table as a sharp boundary, fully saturated below the water table and completely unsaturated above. Variations to the hydraulic conductivity above the water table based on proximity to the water table (Doherty, 2001) do not change the sharp boundary approximation for specific yield.

Replacing SS_i by SY_i in (26) ignores a difference between specific storage and specific yield. I find a conceptual sleight of hand helps illustrate the difference. The concept of a physical change in the void space is replaced by the concept of fluid creation or annihilation. The concept is consistent with the phrase "water coming out of storage" that is often used to describe the effects of specific storage. The equations of flow would be identical if instead of a decrease in void space an equivalent increase in the volume of fluid occurred. With respect to specific storage, this source of creation and removal of water would be distributed throughout the cell volume. To approximate the effect with a node at the center of the cell is appropriate.

In the case of specific yield, the change in available void space to the fluid all occurs above the water table, approximated in a fully saturated flow code as a distinct boundary. For a change in the water table position, the

fluid source should be positioned at the water table for it is there that the change in void space occurs. Approximating the source at the center of the cell introduces an unnecessary error.

We now look at the impact of positioning a node at the water table on the equations of flow for cells that include the water table. Figure 8 depicts three cells. The water table is represented by the dashed line in the upper cell. Large dots are placed at the center of each cell. A circle is located at the center of the water table within the upper cell. For a change in the head of the middle cell, the head dynamics of the top cell are dominated by the flow across the boundary between the two cells balanced by the creation of water at the water table. Location of the cell node is incorporated in the vertical conductance of the upper cell. If the node is located at the center of the cell, then

$$C_{v1}^{c} = \frac{\Delta c \Delta r K_{v1}}{\frac{\Delta z_1}{2}} \tag{29}$$

The superscript c refers to the node at the center of the cell. K_{v1} is the vertical hydraulic conductivity of cell 1. A superscript wt is used to indicate the node at the water table. If the node is located at the water table then

$$C_{v1}^{wt} = \frac{\Delta c \Delta r K_{v1}}{z_{wt} - \left(z_2 + \frac{\Delta z_2}{2}\right)} \tag{30}$$

or

$$C_{v1}^{wt} = \frac{\Delta c \Delta r K_{v1}}{h_1 - \left(z_2 + \frac{\Delta z_2}{2}\right)} \tag{31}$$

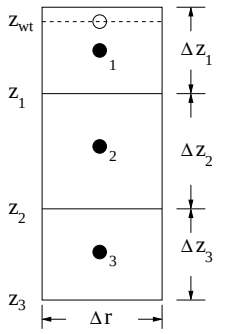

Figure 8: Cells with water table.

If the water table exists at the top of the cell then (31) becomes

$$C_{v1}^{wt} = \frac{\Delta c \Delta r K_{v1}}{\Delta z_1} \tag{32}$$

$$= \frac{C_{v1}^{c}}{2} \tag{33}$$

Likewise, the conductance between the upper and middle cells can be related as

$$C_{v12}^{wt} = \frac{1}{2} \frac{C_{v1}^{c} + C_{v2}}{\frac{C_{v1}^{c}}{2} + C_{v2}} C_{v12}^{c} \tag{34}$$

For the case of $\Delta z_1 = \Delta z_2$ and $K_{v1} = K_{v2}$,

$$C_{v12}^{wt} = \frac{2}{3} C_{v12}^{c} \tag{35}$$

For Figure 8, if the water table is near the bottom of the cell rather than near the top, the conductance between nodes 1 and 2 becomes

$$C_{v12}^{wt} = 2 C_{v12}^{c} \tag{36}$$

4.3 Implementation

Only a small change in coding is needed to implement a water-table-following node. In the subroutine SGF1LPF1VCOND (gwf1lpf1.f), the variable BOVK1 represents $\frac{L}{K_v}$ for the upper cell which we can relate to (29) by $C_{v1}^{c} = \frac{\Delta c \Delta r}{\text{BOVK1}}$. The calculation of BOVK1 changes from

```
BOVK1 = 0.5*(BOTM((J,I,LBOTM(K)-1)-BOTM((J,I,LBOTM(K)))/HYC1
```

for a normal cell, to

```
BOVK1 = (HNEW(I,J,K)-BOTM((J,I,LBOTM(K)))/HYC1
```

when the head (HNEW) in the cell is less than the top of the cell (BOTM((J,I,LBOTM(K)-1)). BOTM((J,I,LBOTM(K))) is the bottom of the cell and HYC1 is the vertical hydraulic conductivity, K_v, of the cell.

4.4 Test Cases

4.4.1 Three-Dimensional Comparison to WTAQ

The influence of the position of the water table node was compared to WTAQ calculations for a hypothetical homogeneous aquifer. The geometry and properties of the aquifer and the positions of the monitoring wells are similar to the Boise Hydrogeophysical Research Site, but the similarity is not significant to this study. The aquifer properties are listed in Table 1.

Parameter	Value
Horizontal K	$1.x10^{-4}$ m/s
Vertical K	$1.x10^{-4}$ m/s
Specific storage	$1.x10^{-4}$ per m
Specific yield	0.38
Aquifer thickness	18 m

Table 1: Aquifer characteristics for the three-dimensional water table modification test.

The pumping well has a radius of 0.0508 m and is screened over an interval of 8 m to 12 m below the water table. Two MODFLOW models using Cartesian geometry are tested. Both have the same 43 rows and 45 columns. The horizontal grid spacing was constructed such that nodes occurred close to the following distances from the pumping well: 3.52 m , 7.08 m, and 22.1 m. One model has 21 layers the other 26. Each layer in the 21 layer model is 1 m thick except for 0.5 m layers above and below each end of the pumping interval, and at the top and bottom of the model. The 26 layer model has a fine grid near the water table. In the 26 layer model, the uppermost layer is 0.1 m thick with eight layers in the upper 3 meters.

Figure 9 presents calculations of drawdown at distances from the pumping well of 3.52 m (well B2), 7.08 m (well C3), and 22.1 m (well X4) at depths of 1 m, 6 m, and 10 m below the water table. Four sets of data are presented in each panel. All of the MODFLOW simulations closely match the WTAQ calculations. The largest deviation between the calculations occurs at nodes closest to the water table and at times when the drawdown is first impacted by the water table decline, causing a brief plateau in the drawdown. After the plateau region the impact of water table decline is fast with respect to the time scale. Figure 10 shows the region of greatest disagreement, the plateau region of the location nearest to the water table and closest to the well. In this figure, the differences between model calculations are clearly presented. The dot-dash line of the 26 layer model is a definite improvement over the dashed line of the 21 layer model. The dotted line of the modified MODFLOW code fails to overlay the WTAQ calculations only at very early times.

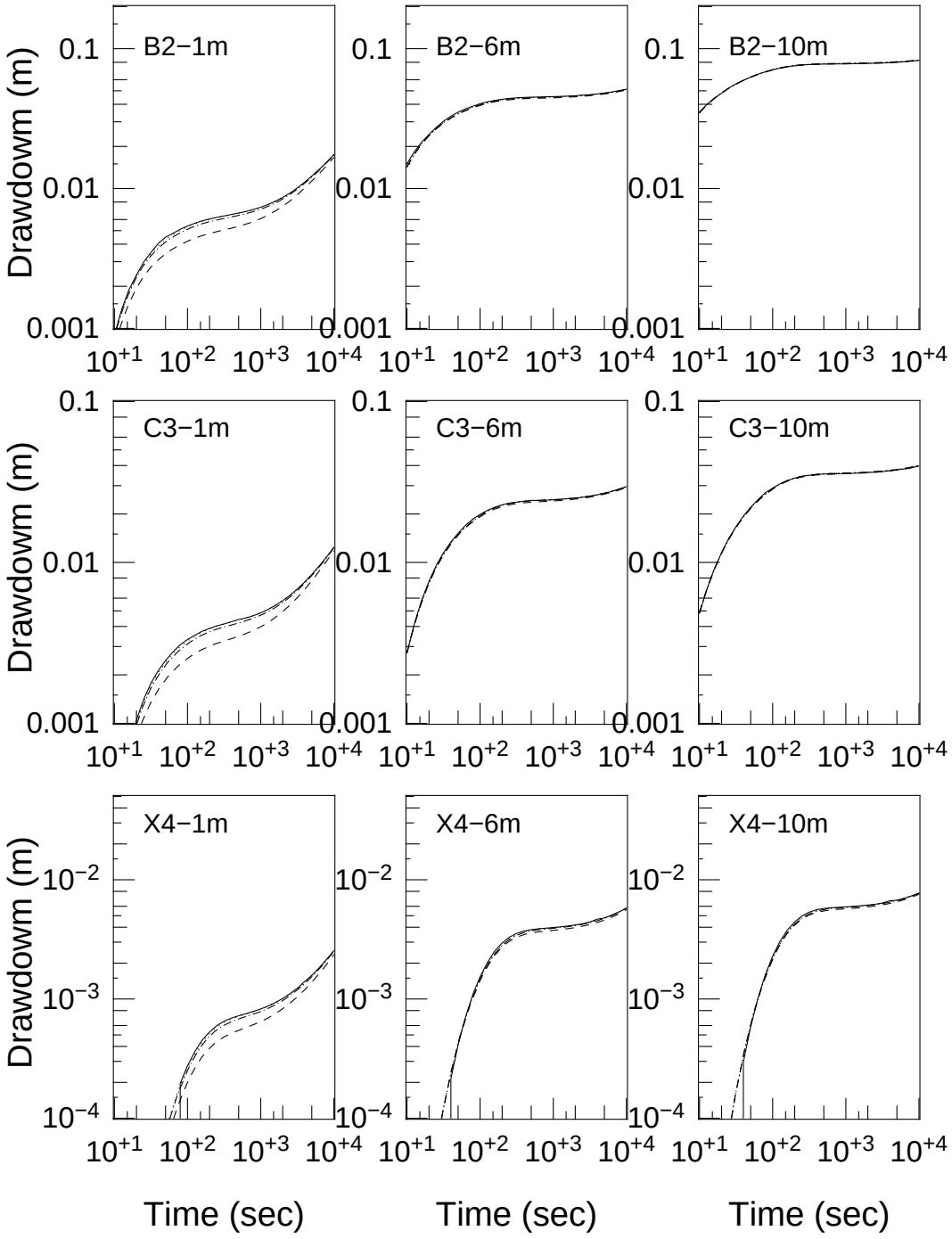

Figure 9: Comparison of drawdown at various locations.

WTAQ calculation (solid), unmodified MODFLOW with 21 layers (dashed), unmodified MODFLOW with 26 layers (dot-dash), modified MODFLOW with 21 layers(dotted). The dotted line overlays the solid line at these scales.

For the test case, the water table modification slows the execution speed of the model by 7%. The increase in layers to 26 compared to 21 layers requires 31% more time to reach a solution.

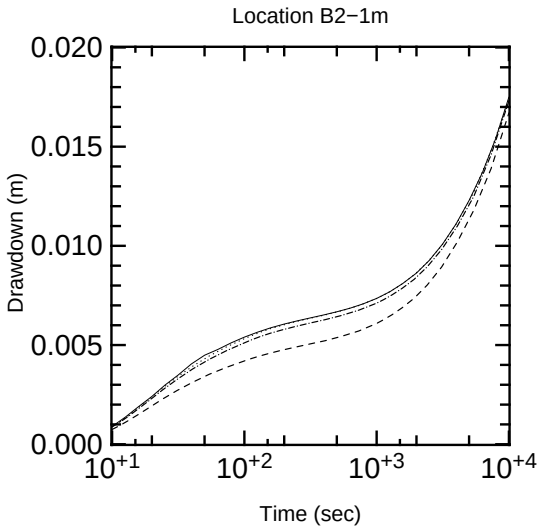

Figure 10: Comparison of drawdown at a depth of 1 m below the water table 3.52 m away from the well. WTAQ (solid), unmodified with 21 layers (dashed), unmodified with 26 layers (dot-dash), and modified with 21 layers (dotted).

4.4.2 Two-Dimensional Cylindrical Geometry Comparison to WTAQ

We use the test case of Section 2.3 for the cylindrical geometry modification. Figure 11 presents the results of the cylindrical geometry test case with the modified water table simulation. WTAQ calculations are presented as a solid line. The cylindrical model calculations, using the center of the uppermost layer as the node position, are shown with a dashed line. The dotted line presents the calculations with the uppermost node following the water table. The three node positions are located by layer and radial column number. For example, Node 3 2 is positioned in Layer 3 Column 2 which translates to 20 ft below the water table and 0.52 ft away from the well.

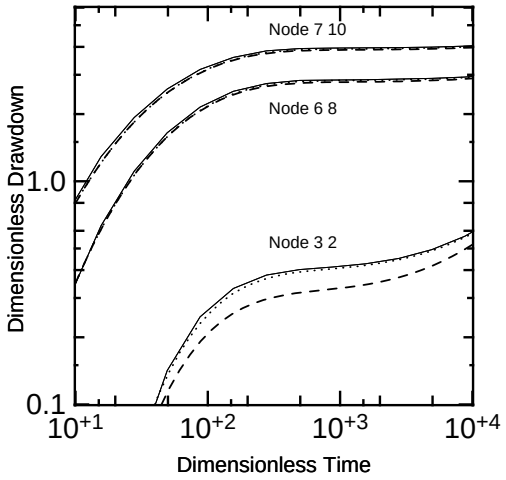

Figure 11: Comparison of WTAQ calculations (solid), cylindrical model without water table modification (dashed), and modified cylindrical model for the RADMOD test case.

5 Limitations of code modifications

This section details the known limitations, and obvious potential limitations, in the current status of our modification to MODFLOW-2000. The limitations are with respect to compatibility with all other packages of MODFLOW-2000. The compatibility to most other packages have yet to be investigated. Incompatibilities that have been identified can be rectified if need be. The need for a FORTRAN 90 or 95 compiler could be removed, but I prefer the present organization of the code.

The layer property flow package has been modified to accommodate cylindrical geometry, but the block-centered flow package has not been modified. The implication of the lack of block-centered flow package compatibility is that the LPF input file must be used rather that the BCF6 input file to describe the material properties in the model. The horizontal flow barrier package has been modified to accommodate cylindrical geometry, but the river, recharge, drain, evapotranspiration, ADV, and general-head boundary packages have not been investigated with respect to compatibility. It is anticipated that none of these packages will be difficult to update for the cylindrical geometry. It may be that most require no changes.

We have not investigated the impact of the water table modification on the sensitivity process. There clearly is an impact that will most likely need to be addressed in a manner similar to the influence of water table variation on horizontal conductance. We intend to address this limitation soon.

6 Summary

This report documents three separate enhancements to the MODFLOW-2000 code: cylindrical geometry, internal flow measurements, and improved water table simulation. The cylindrical geometry enhancement allows the use of the observation, sensitivity and parameter estimation capabilities of MODFLOW-2000 to be applied to situations where radial symmetry can be assumed. Potential uses of cylindrical geometry are the simulation of aquifer dynamics, estimation of the influences of disturbed zones around a wellbore, determination of flow splits into layers that can be applied to larger scale simulations, and our intended use - the interpretation of borehole flow meter data.

The addition of internal flow observations to the observation, sensitivity and parameter estimation processes is a relatively minor enhancement. In addition to simulation of flows for parameter estimation, the simulated observations could useful as an alternative to obtaining flow rates from the cell-by-cell flow file. The enhancement is needed for our intended investigation of borehole flowmeter interpretation.

Our change in water table simulation will improve the performance of any MODFLOW simulation when water table dynamics are important. This improvement has been explained in terms of the process of water table rise and drainage. In the limited test cases we have run, the modifications lead to instability in the model equations that resulted in less than a 10% increase in computation time and in noticeable improvement in accuracy.

7 Acknowledgments

This work was supported by U.S. Army Research Office grants DAAH04-96-1-0318 and DAAD19-00-1-0454 and EPA grant X-970085-01-0.

References

Barlow, Paul M. and Allen F. Moench, 1999. WTAQ-A Computer Program for Calculating Drawdowns and Estimating Hydraulic Properties for Confined and Water Table Aquifers. Water Resources Investigations Report 99-4225, U.S. Geological Survey, Northbough, MA.

Barrash, W., T. Clemo, and M.D. Knoll, 1999. Boise Hydrogeophysical Research Site (BHRS): Objectives, design, initial geostatistical results. In Powers, Micheal H., Lynn Cramer, and Ronald S. Bell, editors, *Proceedings of the Symposium on the Application of Geophysics to Engineering and Environmental Problems, Oakland, CA*, pages 389–398, 10200 W. 44th Ave. #304 Wheat Ridge, CO. Environmental and Engineering Geophysical Society.

Doherty, John, 2001. Improved calculations for dewatered cells in MODFLOW. *Groundwater*, 39(6):863–869.

Harbaugh, A.W., E.R. Banta, M.C. Hill, and M.G. McDonald, 2000. MODFLOW-2000, the U.S. Geological Survey modular ground-water model – User guide to modularization concepts and the Ground-Water Flow Process. Open File Report 00-92, U. S. Geological Survey, Denver, CO.

Hill, M.C., E.R. Banta, A.W. Harbaugh, and E.R. Anderman, 2000. MODFLOW-2000, the U.S. Geological Survey Modular Ground-Water Model – User guide to the Observation, Sensitivity, and Parameter-Estimation Processes and Three Post-Processing Programs. Open File Report 00-184, U. S. Geological Survey, Denver, CO.

Johnson, Gary S., Davis B. Frederick, and Donna M. Cosgrove, 2002. Evaluation of a pumping test of the Snake River Plain aquifer using axial-flow numerical modeling. *Hydrogeology Journal*, 10(3):428–437.

Moench, Allen F., 1997. Flow to a well of finite diameter in a homogeneous, anisotropic water table aquifer. *Water Resources Research*, 33(6):1397–1407.

Molz, F.J., G.K. Boman, S.C. Young, and W.R. Waldrop, 1994. Borehole flowmeters: Field application and data analysis. *Journal of Hydrology*, (163):347–371.

Neuman, Shlomo P., 1974. Effect of partial penetration on flow in unconfined aquifers considering delayed gravity response. *Water Resources Research*, 10(2):303–311.

Reilly, Thomas E. and Arlen W. Harbaugh, 1993. Computer Note: Simulation of cylindrical flow to a well using the U.S. Geological Survey modular finite-difference ground-water flow model. *Ground Water*, 31(3):489–494.

Tera Analysis, 1999. *Quickfield, Version 4.2.* Tera Analysis Company, P. O. Box 571086 Tarzana, CA 91357.

Young, Steven, C. and Hubert S. Pearson, 1995. The electromagnetic borehole flowmeter: Description and application. *Ground Water Monitoring & Remediation*, 15(4):138–147.

A Appendix A

Input Instructions

A.1 Input instructions for inner boundary of radial geometry

The file contains a single number, the distance of the inner boundary of the radial cross-section from the axis of symmetry. The file name is specified in the name file using file type designation CGEO.

0. [text]

   Item 0 is optional and can include as many lines as needed.

   Each line must contain the # character in first column.

1. SR1 (free format)

Explanation of Variables

text is a character string of up to 79 characters that starts in column 2.

SR1 is the distance from the axis of symmetry in the cylindrical geometry to the inner boundary of Column 1. The column widths are defined by DELR of the DIS file. The columns progress outward from SR1.

A.2 Input instructions for internal flow observations

Input instructions for the internal flow package are read from a file specified with FLOB as the file type in the name file.

0. [#text]

   Item 0 is optional and can include as many lines as needed. Each line contains the # character in first column.

1. NQFL NQCFL NQTFL (free format)

2. TOMULTFL EVFFL IOWTQFL (free format)

   Read items NQTFL,4, and 5 for each NQFL groups of cells for which internal flow observations are to be specified.

3. NQOBFL NQCLFL (free format)

   Read item 4 for each NQOBFL observation times for this group of cells. STATISTIC and STAT-FLAG are ignored if IOWTQFL is greater than zero.

4. OBSNAM IREFSP TOFFSET HOBS STATSTIC STAT-FLAG PLOT-SYMBOL (free format)

   Read item 5 for each of |NQCLFL|cells in this group.

5. TO_LAYER TO_ROW TO_COL FR_LAYER FR_ROW FR_COL FACTOR (free format)

   Read items 6 and 7 if IOWTQFL is greater than zero.

6. FMTIN IPRN (free format)

7. WTQ(1,1), WTQ(1,2), WTQ(1,NQTFL), ..., WTQ(1,NQTFL) (format: FMTIN)
   WTQ(2,1), WTQ(2,2), WTQ(2,NQTFL), ..., WTQ(2,NQTFL)

   ⋮

   WTQ(NQTFL,1), WTQ(NQTFL,2), WTQ(NQTFL,3), ..., WTQ(NQTFL,NQTFL)

Explanation of Variables

text is a character string of up to 79 characters that starts in column 2.

NQFL is the number of cell groups for which internal flow observations are listed. A group in a collection of cell pairs that define an internal surface that represents the location of a single flow measurement.

NQCFL is greater than or equal to the total number of cells in all cell groups. NQCFL must be greater than or equal to the sum of all |NQCLFL|

NQTFL is the total number of internal flow observations for all cell groups. NQTFL must equal the sum of all NQOBFL, which are specified in repetitions of item 3.

TOMULTFL is the time offset multiplier for the observations. The product of TOMULTFL and TOFFSET must produce a time value in units consistent with other model input. TOMULTFL can be dimensionless or can be used to convert the TOFFSET units.

EVFFL is the error variance multiplier for internal flow observations. It is used to calculate the weights as described in the STATSTIC explanation.

IOWTQFL indicates whether the variance-covariance matrix is to be read for the internal flow observations as item 7. If IOWTQFL is greater than zero, then the variance-covariance matrix is read and used to calculate the weights. If IOWTQFL is zero, the matrix is not read and STATISTIC is used.

NQOBFL is the number of times at which flows are observed for the group of cells.

NQCLFL is used for two purposes. The absolute value of NQCLFL is the number of cell pairs in the group. If NQCLFL is negative then FACTOR is forced to 1.0 for all cells in the group, otherwise FACTOR is read for each cell pair in item 5.

OBSNAM is a 1 to 12 character string used to identify the observation. OBSNAM may not contain internal white-space characters.

IREFSP is the reference stress period to which the observation time is referenced. The reference time is the beginning of the stress period.

TOFFSET is the time from the beginning of the stress period IREFSP to the time of the observation. The multiplier TOMULTFL allows TOFFSET to be in units other than the units of the simulation.

HOBS is the observed volumetric flow rate across the boundary defined by the group of to and from cell pairs.

STATISTIC is the value from which the weight for the observation is calculated. STAT-FLAG controls the calculation as described below. STATIC is ignored if the variance-covariance matrix is used (IOWTQFL>0).

STAT-FLAG controls how STATICSTIC is used. If IOWTQFL>0 then STAT-FLAG is ignored

STAT-FLAG=0 => STATISTIC is a scaled standard variance $\left[\left(\frac{L^3}{T}\right)^2\right]$

weight = $\frac{1}{(STATISTIC*EVFFL)}$

STAT-FLAG=1 => STATISTIC is a scaled standard deviation $\left[\frac{L^3}{T}\right]$

weight = $\frac{1}{(STATISTIC^2*EVFFL)}$

STAT-FLAG=2 => STATISTIC is a scaled coefficient of variation [ ]

weight = $\frac{1}{(STATISTIC*HOBS)^2*EVFFL}$

PLOT-SYMBOL is an integer that will be written to the output files intended for graphical analysis to allow control of the symbols used when plotting data.

TO-LAYER is the layer of the recieving cell. Positive flow is toward the recieving cell and away from the discharging cell. TO-LAYER and FR-LAYER define the layer boundary across which the simulated flow measurement is calculated.

TO-ROW is the row of the recieving cell. TO-ROW and FR-ROW define the row boundary used to calculate the simulated flow measurement.

TO-COL is the column of the recieving cell. TO-COL and FR-COL define the column boundary used to calculate the simulated flow measurement.

FR-LAYER is the layer of the discharging cell.

FR-ROW is the row of the discharging cell.

FR-COL is the column of the discharging cell.

FACTOR is the fraction of the calculated flow added to the flow measurement.

FMTIN is the format used to space the variance-covariance matrix data listed in item 7. The format is a FORTRAN specification for REAL numbers and must be enclosed in parentheses.

IPRN identifies the format used in printing the variance-covariance matrix. If IPRN is less than 1 the matrix is not printed.

Output requires more than 80 columns		Output fits in 80 columns	
IPRN	FORMAT	IPRN	FORMAT
1	10G12.3	6	5G12.3
2	10G12.4	7	5G12.4
3	9G12.5	8	5G12.5
4	8G13.6	9	4G13.6
5	8G13.7	10	4G13.7

Table 2: IPRN format specifications

WTQ Is an NQTFL by NQTFL array containing the variance-covariance array for the internal flow measurements in units of $\left[\frac{L^3}{T^2}\right]$. All elements of the matrix must be entered.